Available online at www.sciencedirect.com
SCIENCE DIRECT®
Journal of Solid State Chemistry 177 (2004) 1078–1086
JOURNAL OF SOLID STATE CHEMISTRY
http://elsevier.com/locate/jssc

Crystal structure and magnetism of layered $Ln_2Ca_2MnNiO_8$ (Ln = Pr, Nd, Sm, and Gd) compounds

Duk-Kyun Han,[a] Sang-Hwan Kim,[a] Kun-Pyo Hong,[a] Young-Uk Kwon,[a,*] Sunghyun Kim,[b] and Jeong-Soo Lee[c]

[a] *Department of Chemistry and BK-21 School of Molecular Science, Sungkyunkwan University, Suwon 440-746 South Korea*
[b] *Department of Chemistry, Konkuk University, Seoul 143-701 South Korea*
[c] *Korea Atomic Energy Research Institute, Daejon 350-600 South Korea*

Received 19 July 2003; received in revised form 9 October 2003; accepted 14 October 2003

Abstract

We report the syntheses, crystal structure, and magnetic properties of a series of distorted K_2NiF_4-type oxides $Ln_2Ca_2MnNiO_8$ (Ln = Pr, Nd, Sm, and Gd) in which Ln/Ca and Mn/Ni atoms randomly occupy the K and Ni sites respectively. The Ln = La compound does not form. These compounds show systematic distortions from the ideal tetragonal K_2NiF_4 structure (space group $I4/mmm$) to an orthorhombic structure (space group $Pccn$) with buckled MO_2 (M = Mn/Ni) layers. The degree of distortion is increased as the size of Ln decreases. Based on the magnetic data and X-ray absorption near edge spectra, we assigned Mn^{IV} and Ni^{II}. The Curie–Weiss plots of the high temperature magnetic data suggest strong ferromagnetic interactions probably due to Mn^{IV}–O–Ni^{II} linkages, implying local ordering of Mn/Ni ions to form ferromangnetic clusters in the MO_2 layers. At low temperatures below 110–130 K, these compounds show antiferromagnetic behaviors because of Mn^{IV}–O–Mn^{IV} and/or Ni^{II}–O–Ni^{II} contacts between the ferromagnetic clusters. The Ln = Pr and Nd compounds show additional antiferromagnetic signals that we attribute to the interlayer interactions between the clusters mediated by the Pr^{3+} and Nd^{3+} ions in the interlayer spaces. The present compounds show many parallels with the previously reported $Ln_2Sr_2MnNiO_8$ compounds.

Keywords: K_2NiF_4; Layered compound; Magnetic property; Crystal structure; Interlayer magnetic interactions

1. Introduction

K_2NiF_4-type oxides show many interesting physical properties such as superconductivity [1], magnetoresistance [2], and spin glass interactions [3,4], probably strongly related with the two-dimensional anisotropy of the structure (Fig. 1a). In most of the layered compounds, the primary assumption is that there are little or no interactions between the layers [5]. However, there have been several reports that suggest interlayer interactions with various types of mechanisms, including magnetic Ln ions and interstitial oxygen in the interlayer space [2,4,6–8]. In their paper on $Ln_{0.7}Sr_{1.3}MnO_4$ (Ln = La–Nd) single crystals, Hong et al. have reported that the magnetic properties of the Pr and Nd compounds are different from the La one in that the former show interlayer magnetic interactions that, in turn, influence the electronic properties of the compounds [4]. Also, we have previously studied a series of compounds $Ln_2Sr_2MnNiO_8$ (Ln = La–Gd) and found that the Pr and Nd compounds show an additional magnetic signal to that of La compound which we explained as an interlayer magnetic interaction [9]. These results strongly indicate that the magnetic ions in the interlayer space of layered compounds may play crucial roles in determining the physical properties.

In this paper, we report the syntheses, crystal structures, and magnetic properties of series compounds $Ln_2Ca_2MnNiO_8$ (Ln = Pr–Gd), Ca analogues of $Ln_2Sr_2MnNiO_8$ compounds. The Ca compounds turn out to have structural deviations from the ideal K_2NiF_4-type structure. Therefore, it would be interesting to compare their structures and magnetic properties of the compounds in the Sr-series.

*Corresponding author. Fax: +82-31-290-7075.
E-mail address: ywkwon@skku.edu (Y.-U. Kwon).

0022-4596/$ - see front matter © 2003 Elsevier Inc. All rights reserved.
doi:10.1016/j.jssc.2003.10.016

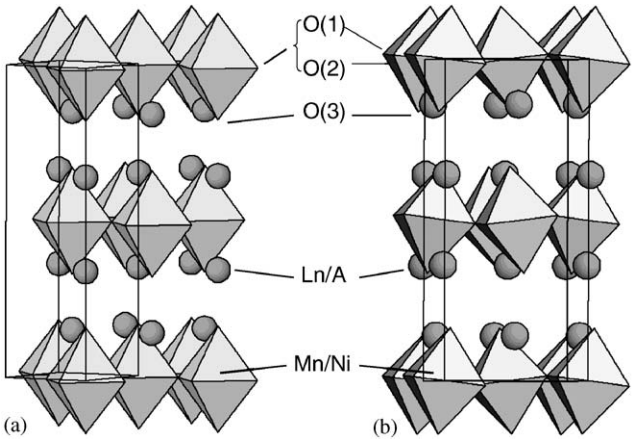

Fig. 1. K_2NiF_4 type structures and labeling scheme (a) in the ideal $I4/mmm$ space group and (b) distorted variation in the $Pccn$ space group.

2. Experimental

Samples of the title compounds were synthesized from the conventional solid-state reactions. Stoichiometric amounts of R_2O_3 (R = Nd, Sm, Gd), Pr_6O_{11}, $CaCO_3$, $MnCO_3$, NiO were ground together, pressed into pellets, and heated at 1400°C for 24 h in air. All the reagents were baked overnight before use.

X-ray powder diffraction data were obtained by using a rotating anode (12 kW) M18XHF-SRA (Mac Science) diffractometer equipped with a CuK_α-radiation ($\lambda = 0.154184$ nm). The data were collected with a step scan method for Rietveld pattern refinements with a step size 0.02 and 10 s per step in the $2\theta = 10-90°$ range.

Room temperature and 10 K powder neutron diffraction experiments for the Nd compound were performed with a HRPD in the research reactor HANARO at Korea Atomic Energy Research Institute (KAERI). Wavelength of 0.18339 nm was selected with a vertically bent Ge(331) monochromator. The data were collected in the 2θ-range 0–160° with 0.05° steps. A vanadium sample holder with 0.1 mm thickness was used to reduce noise. The detector efficiency was corrected based on a separate experimental result.

Rietveld refinements on the X-ray powder diffraction patterns were performed with the Fullprof program [10]. Absorption corrections, pseudo-Voigt profile function, five background parameters and asymmetric peak shape functions were used for the refinements. The $K_{\alpha 2}/K_{\alpha 1}$ ratio was fixed at the theoretical value of 0.5 in all refinements.

X-ray Absorption Near-Edge Spectroscopic (XANES) measurements in a transmission mode were carried out at line 3C1 of Pohang light source (PLS) and line 7C of photon factory (PF), operating at an energy of 2.05 and 2.5 GeV with ring current of ca. 100–200 and 200–400 mA, respectively. The monochromatic beam was obtained by a Si(111) double crystal that was detuned by 30% to reject higher harmonics. In the XANES region, the energy was scanned with an increment of 0.3 eV. The vertical slit width was adjusted less than 1 mm for a better energy resolution. The energy calibration was done using metallic foils of three-absorption lengths. The first inflection points were taken as E_0 (6539 eV for Mn and 8333 eV for Ni) and used to calibrate all the data.

Magnetic measurements were performed on a SQUID in the temperature range 5–300 K for both field cooled (FC) and zero field cooled (ZFC) runs. Measurements were made both under 100 and 5000 G of magnetic field strengths.

3. Results and discussion

3.1. Structure and synthesis

The XRD patterns of all the four (Ln = Pr–Gd) compounds show the characteristic features of a K_2NiF_4 type structure (Fig. 2). However, on close inspection, one finds that the peaks are systematically broadened or split depending on the reflection indices and Ln ions. This is well exemplified by the peaks at $2\theta = 32-34°$ regions: The (110) peak of the Pr compound becomes broad on moving to Nd and Sm compounds and split in the Gd compound, while the width of the (103) peak does not seem to change with Ln, indicating symmetry lowering from the ideal tetragonal K_2NiF_4 structure to an orthorhombic structure. The degree of peak broadening increases with the decrease of the Ln ionic size.

In order to account for the lower symmetry of the Gd-compound, we have tried Rietveld structure refinements with several models in the orthorhombic crystal system and found that the model in the $Pccn$ space group explains the observed XRD pattern well. The $Pccn$ derivative structure has been reported for Sr_2SnO_4 [11] and $La_2NiO_{4+\delta}$ [12]. Also, many of the superconductor cuprate compounds $Ln_{2-x}A_xCuO_4$ (Ln = rare earth, A = alkaline earth) are reported to have this structure at low temperatures [13]. In the ideal K_2NiF_4 structure the MO_6 octahedron has a local symmetry D_{4h} with four short equatorial M–O bonds in the ab-plane and two long axial M–O bonds. In the $Pccn$ variation, the four-fold symmetry is broken and the local symmetry becomes D_{2h} with three pairs of inversion-related M–O bonds while maintaining the O–M–O bond angles at 90° (Fig. 1b). The perfectly planar MO_2 plane in the ideal K_2NiF_4 structure becomes buckled with the equatorial oxygen atoms alternatively above and below the plane of M ions. However, this symmetry lowering is not sufficient to explain the details of the diffraction pattern as can be seen in Fig. 3a. When the refinements were

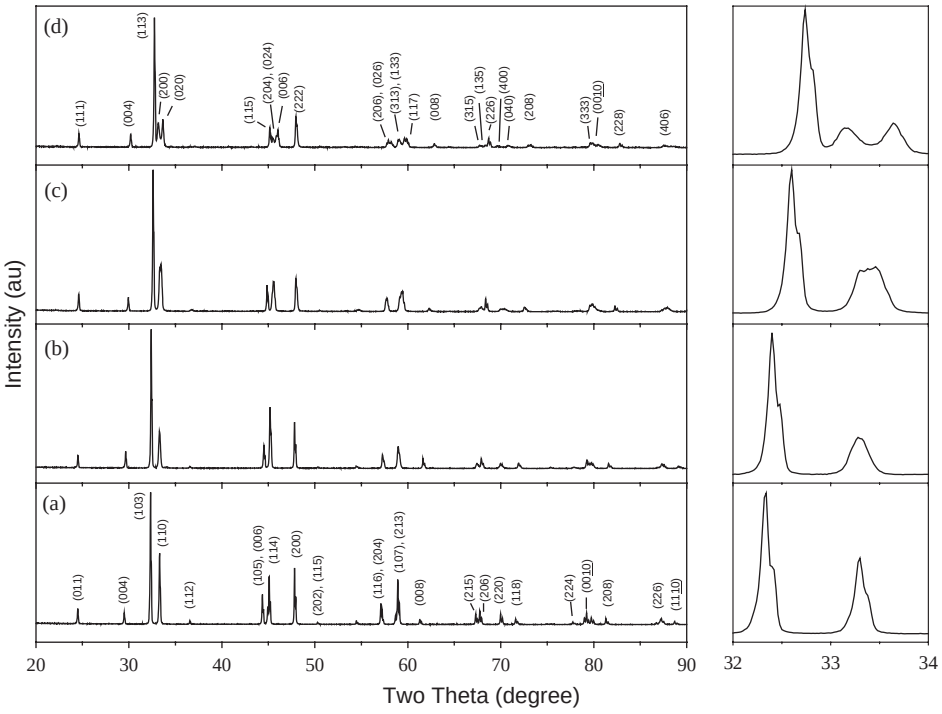

Fig. 2. X-ray powder diffraction patterns of $Ln_2Ca_2MnNiO_8$ compounds: (a) Ln = Pr, (b) Nd, (c) Sm, and (d) Gd. In the right-hand side panel the $2\theta = 32-34°$ regions are shown. The structural refinements were performed with the space group *Pccn* and the indices are given in (d). The tetragonal indices given in (a) are for comparison purpose only.

performed with isotropic temperature factors, the split peaks, (200) and (020), show poor agreement with the observed pattern. This is somewhat improved when the temperature factors were refined anisotropically (Fig. 3b). However, considering the drastically increased number of parameters in the anisotropic model, the improvement of the fit may be discounted. This problem could be alleviated considerably when a strain model [14] with fluctuations along the *a*- and *b*-directions was employed in the refinements as shown in Fig. 3c. These fluctuations might be because of the different ionic sizes of Mn and Ni ions that are randomly distributed in the *M* sites. In our previous paper, we have reported that the $Ln_2Sr_2MnNiO_8$ (Ln = La–Gd) compounds all adopt the ideal tetragonal structure. Probably, the substitution of Sr with Ca makes the average size of *Ln*/Ca ion too small to match the size of Mn/Ni–O framework and makes the latter to distort.

With the results of $Gd_2Ca_2MnNiO_8$ compound, the XRD data of the other compounds with larger *Ln*'s were also refined with the *Pccn* model. The Sm compound with split peaks undoubtedly is under the same effect but to a lesser degree. The Nd-compound is also distorted with the peak at $2\theta = 33°$ broader than that in the Pr compound. Although the Pr-compound does not seem to have the orthorhombic distortion judging from the peak shape and width only, the refinements with the orthorhombic model ($R_p = 8.60$, $R_{wp} = 11.2$) produced a better fit than the one with the tetragonal model ($R_{p=}10.5$, $R_{wp} = 13.1$). In Tables 1 and 2, the crystallographic data and selected bond distances and angles are listed, respectively.

The two equatorial *M*–O bonds (*M*–O(1) and *M*–O(2)) of Pr–Sm compounds have almost the same bond distances despite the low symmetry and these values are held constant at 1.90 Å within standard deviations. In the Gd compound, however, these bond distances are significantly different from each other although their average remains unchanged at 1.90 Å. On the other hand, the axial *M*–O(3) bond distance shows a gradual decrease on moving from Pr through Gd compounds. The *M*–O–*M* bond angles, in average, also show a gradual decrease from 175° for Pr and Nd compounds to 167° for Gd compound.

In contrast to the analogous $Ln_2Sr_2MnNiO_8$ series, we could not synthesize Ln = La compound as a single phase. The products of the attempted syntheses all showed many extra peaks in addition to the desired K_2NiF_4 type peaks. This indicates that there is a K_2NiF_4 type phase in the $(La,Ca)_2(Mn,Ni)O_4$ system, but the proportions of La/Ca and/or Mn/Ni are different from the loaded composition. This may be because that the La/Ca ionic size and the Mn/Ni–O framework do not produce a good fit to form a single phase. Similar observations were made in the $Ca_{2-x}Ln_xMnO_4$ system in which the Ln = La compound did not form while the Ln = Pr–Gd compounds formed [15].

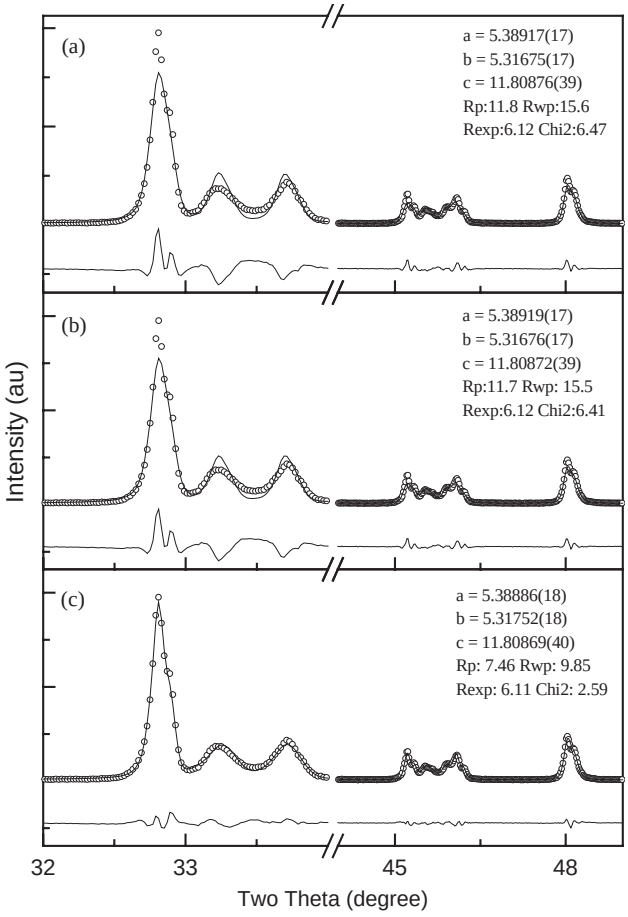

Fig. 3. Rietveld refinements of the $Gd_2Ca_2MnNiO_8$ compound with various models in *Pccn* space group: (a) No strain and isotropic temperature factors, (b) no strain and anisotropic temperature factors, and (c) strain and isotropic temperature factors.

3.2. XANES spectroscopy and magnetism

In our previous paper, we have reported that $Ln_2Sr_2MnNiO_8$ (Ln = La–Gd) compounds have several interesting features: (a) The transition metal atoms have oxidation states Mn^{IV} and Ni^{II} based on XANES spectroscopic data and magnetic moment data compared with several models of various oxidation states of the transition metal atoms. (b) These M ions are ordered in short ranges and the positive superexchange interaction energy [16] of 180° Mn^{IV}–O–Ni^{II} linkages give rise to ferromagnetic regions or clusters within the MO_2 layers with Weiss temperatures of 46–84 K. (c) Neighboring ferromagnetic clusters interact antiferromagnetically because of Mn^{IV}–O–Mn^{IV} and Ni^{II}–O–Ni^{II} bonds between them that have negative superexchange energies [16]. This intralayer inter-cluster antiferromagnetic interaction sets in below 105–126 K depending on the nature of Ln ion. (d) For Pr and Nd compounds, there is an additional antiferromagnetic ordering below 78–80 K, which is attributed to M–O–Ln–O–M interlayer interaction. The present $Ln_2Ca_2MnNiO_8$ compounds show many parallels with the Sr-analogues of corresponding Ln as detailed in the following.

The oxidation states of the Mn and Ni ions were determined by XANES spectroscopic studies. Figs. 4 and 5 show the normalized (panel A) and first differential (panel B) Mn and Ni K-edge XANES spectra, respectively, for our samples and reference compounds. We have used the dipole-forbidden but quadrupole-allowed $1s \rightarrow 3d$ transition peak positions in the determination of oxidation states of absorbing atoms [17]. For the oxidation state of Mn, we have used Mn_2O_3 as the reference for +3 state and MnO_2, Ca_2MnO_4, and $LaMn_{0.5}Ni_{0.5}O_3$ as the references for +4 state. Two $1s \rightarrow 3d$ peaks, labeled as A_1 and A_2 in Fig. 4, are ascribed to electronic transitions to the final states with t_{2g} and e_g symmetries, respectively. The position of A_1, marked with asterisks, served as an indicator of the oxidation state [18]. The references show that this peak appears at 6539.5 eV for Mn^{III} and 6540.0 eV for Mn^{IV}. All of our samples show this peak at 6539.9–6540.1 eV, suggesting Mn oxidation states of +4. The Sr-analogues also showed this peak at 6540.0 eV [9].

Similar arguments may also apply to the determination of Ni oxidation states. The $1s \rightarrow 3d$ transitions for Ni^{II} references (NiO and $LaMn_{0.5}Ni_{0.5}O_3$) appear at 8332.0 eV and for Ni^{III} references (NiOOH and $LaSrNiO_4$) at 8333.0 eV. Unlike the Mn spectra, the Ni spectra show that the peak position is lowered as the size of Ln decreases. In the $Ln_2Sr_2MnNiO_8$ system, this peak appears at 8331.8–8332.4 eV, close to the value of Ni^{II} than Ni^{III}. However, in the present system, the Pr sample shows a peak at 8332.8 eV, closer to the value of Ni^{III}, while the others show peaks at 8332.2–8332.4 eV, closer to the value of Ni^{II}. It is not clear why the Ni in the Pr compound shows a XANES peak close to Ni^{III}. One possible cause is the presence of impurity (to be discussed below in the magnetism). Also it is possible that there are interstitial oxygen atoms in this compound to induce the oxidation of Ni [8,19]. However, the impure sample state prohibited any further pursuit to understand the unusually large absorption peak energy of this compound. With the XANES spectroscopic data we could assign the oxidation states of the compounds in the present study as Mn^{IV} and Ni^{II} except for the uncertainty of the Ni in the Pr compound. The results are summarized in Table 3. These oxidation states are also consistent with the effective magnetic moments calculated from the Curie–Weiss fits of the magnetic susceptibility data (see below).

The magnetic susceptibility and inverse magnetic susceptibility data as functions of temperature for all compounds are shown in Fig. 6. Despite the structural distortions described above, the magnetic properties of the present compounds resemble those of the $Ln_2Sr_2MnNiO_8$ (Ln = La–Gd) compounds with

Table 1
Reitveld refinement results for $Ln_2Ca_2MnNiO_8$ (Ln = Pr, Nd, Sm, Gd) compounds

	Pr	Nd	Sm	Gd
a (Å)	5.3625(2)	5.3568(1)	5.3673(1)	5.3889(2)
b (Å)	5.3663(2)	5.3747(1)	5.3405(1)	5.3175(2)
c (Å)	12.0857(1)	12.0182(2)	11.9038(1)	11.8087(4)
V (Å^3)	347.79(2)	346.02(1)	341.21(1)	338.38(3)
Ln/Ca, 8e (x, y, z)				
x	0.0017(19)	−0.0002(9)	0.0061(6)	0.0132(3)
y	−0.0005(34)	−0.0049(7)	−0.0017(7)	0.0013(18)
z	0.35871(6)	0.35930(6)	0.35907(9)	0.35941(7)
U_{iso} (Å^2)	0.762(17)	0.865(2)	1.71(2)	1.98(3)
Mn/Ni, 4a (000)				
U_{iso} (Å^2)	0.65(4)	0.59(5)	2.21(6)	2.42(7)
O1, 4d (1/4, 3/4, z)				
Z	0.0001(254)	0.0028(69)	0.0137(24)	0.0060(28)
U_{iso} (Å^2)	1.147(999)	−0.02(55)	0.18(53)	2.421(67)
O2, 4c (1/4, 1/4, z)				
Z	0.0131(33)	−0.0089(38)	0.0121(35)	0.0218(20)
U_{iso} (Å^2)	0.512(999)	3.42(94)	4.18(87)	1.78(20)
O3, 8e (x, y, z)				
X	−0.003(49)	0.0251(37)	−0.0134(41)	−0.0331(23)
Y	0.0257(69)	0.0285(38)	0.0373(26)	0.002(11)
Z	0.1735(5)	0.1723(5)	0.1700(7)	0.1667(6)
U_{iso} (Å^2)	1.98(25)	1.13(24)	2.46(20)	4.38(20)
Strain parameters[a]				
σ_a			13.0(3)	24.6(3)
σ_b			16.6(3)	22.5(3)
Corr(ab)			−0.55(3)	−0.76(2)
Reliability factors				
R_P	8.44	8.35	6.18	7.46
R_{WP}	11.0	10.8	8.23	9.85
R_{EXP}	11.44	11.19	4.47	6.11
χ^2	0.931	0.937	3.39	2.59

$FWHM^2 = 3.2 \times 10^{-2}(\ln 2)\tan\theta\{\sigma_a^2(h/a)^4 + \sigma_b^2(k/b)^4 + 2\mathrm{corr}(ab)\sigma_a\sigma_b(h/a)^2(k/b)^2\}/\{(h/a)^2 + (k/b)^2 + (l/c)^2\}$.

[a] Strain parameters for the orthorhombic fluctuation of a and b parameters.

Table 2
Important bond distances and angles of $Ln_2Ca_2MnNiO_8$ (Ln = Pr, Nd, Sm, Gd) compounds

	Pr	Nd	Sm	Gd
Ln/A–O(1)	2.56(6)	2.53(6)	2.45(2)	2.51(2)
	2.55(7)	2.55(6)	2.62(2)	2.53(2)
Ln/A–O(2)	2.45(3)	2.60(3)	2.45(3)	2.40(1)
	2.66(3)	2.49(3)	2.62(3)	2.66(2)
Ln/A–O(3)	2.243(7)	2.259(7)	2.263(9)	2.289(8)
	2.57(2)	2.54(2)	2.49(1)	2.68(3)
	2.69(2)	2.84(2)	2.61(2)	2.46(1)
	2.74(2)	2.57(2)	2.82(2)	2.96(1)
	2.85(2)	2.90(2)	2.90(1)	2.68(3)
Mn/Ni–O(1) × 2	1.897(3)	1.897(2)	1.900(2)	1.894(1)
Mn/Ni–O(2) × 2	1.903(2)	1.900(2)	1.898(3)	1.910(3)
Mn/Ni–O(3) × 2	2.101(7)	2.081(6)	2.035(9)	1.977(8)
M–O(1)–M	180	178	170	165
M–O(2)–M	170	174	171	169

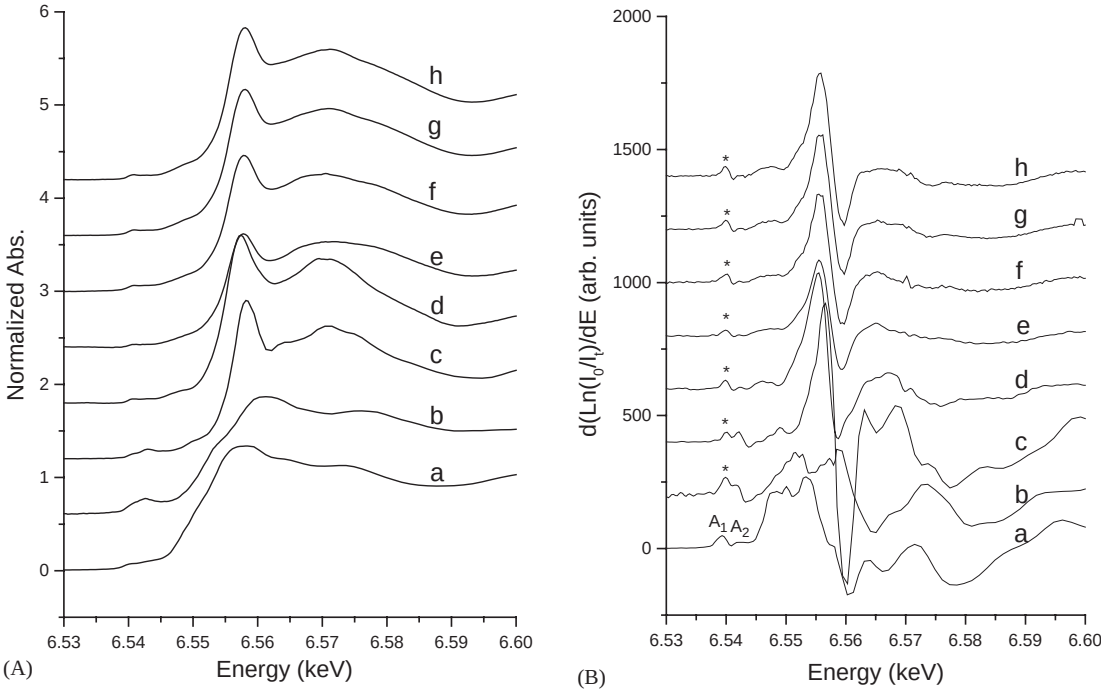

Fig. 4. Normalized (panel A) and first differential (panel B) XANES spectra of Mn for (a) Mn_2O_3, (b) MnO_2, (c) Ca_2MnO_4, (d) $LaMn_{0.5}Ni_{0.5}O_3$, (e) $Pr_2Ca_2MnNiO_8$, (f) $Nd_2Ca_2MnNiO_8$, (g) $Sm_2Ca_2MnNiO_8$, (h) $Gd_2Ca_2MnNiO_8$. $1s \rightarrow 3d$ transition (A_1 peak) is labeled by an asterisk (*).

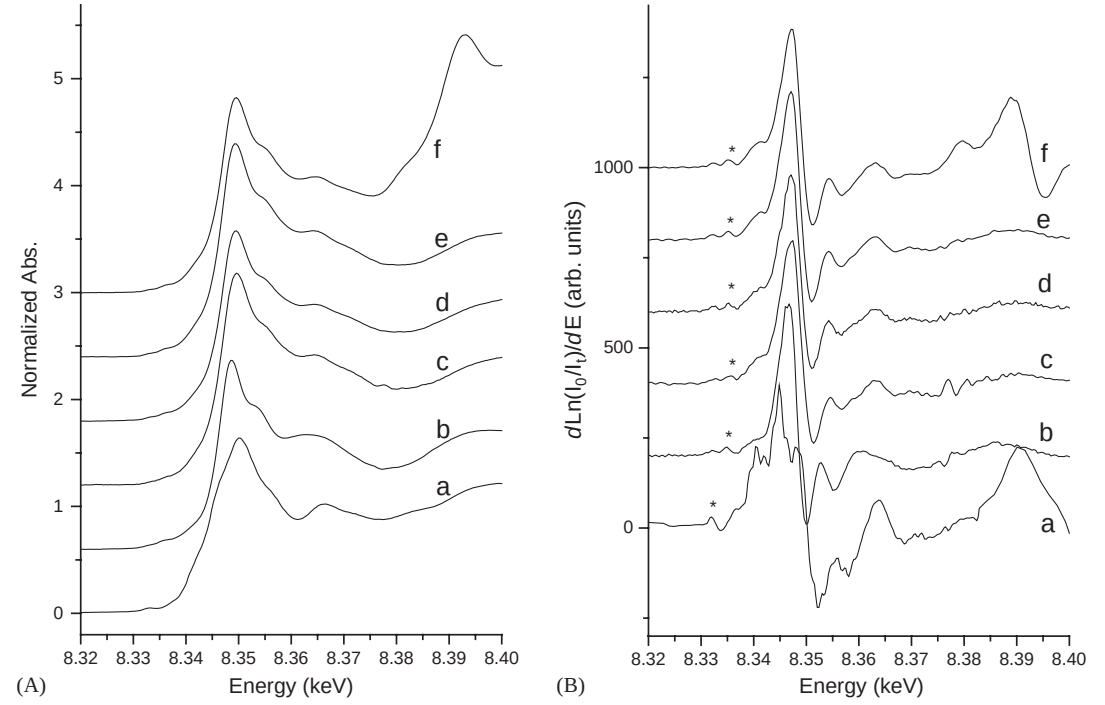

Fig. 5. Normalized (panel A) and first differential (panel B) XANES spectra of Ni for (a) NiO, (b) $LaMn_{0.5}Ni_{0.5}O_3$, (c) $Pr_2Ca_2MnNiO_8$, (d) $Nd_2Ca_2MnNiO_8$, (e) $Sm_2Ca_2MnNiO_8$, (f) $Gd_2Ca_2MnNiO_8$. $1s \rightarrow 3d$ transition is labeled by an asterisk (*).

one-to-one correspondence between those with the same *Ln* (Table 4). The Pr compound shows a discrepancy between ZFC and FC data up to 180 K while the others show such deviations at much lower temperatures. The deviation above 120 K of the Pr compound appears to arise from impurities, considering that the Pr compound of the Sr-series does not show such a high temperature deviation. However, these data are almost the best among those of other Pr compound samples we have synthesized suggesting that the impurities are an

inherent problem of the Pr-compound probably because the Pr/Ca and Mn/Ni ratios of the K_2NiF_4 phase are slightly different from the loaded values. The fact that we have failed to synthesize the La-compound supports this possibility.

The lack of any superstructure reflections in the X-ray and neutron diffraction patterns indicates that the Mn^{IV} and Ni^{II} ions of the MO_2 layer are not ordered in a long range scale. However, we believe that the sharp differences in their sizes and charges induce some local ordering. From electron diffraction studies on related compounds, $La_2Sr_2BMnO_8$ (B = Mg, Zn), Burley et al. reported that the *B* and Mn atoms were short-range ordered within the *ab*-plane [20]. The ferromagnetism of the 3D version of our compounds, Ln_2MnNiO_6, was explained with the ordering of Mn^{IV} and Ni^{II} ions and their ferromagnetic superexchange interactions [21].

With Mn^{IV} and Ni^{II} ions randomly distributed, there are three possible magnetic superexchange interactions; Mn^{IV}–O–Mn^{IV}, Ni^{II}–O–Ni^{II}, and Mn^{IV}–O–Ni^{II}. The first two are antiferromagnetic and the third one ferromagnetic. If Mn^{IV} and Ni^{II} are perfectly ordered, only the third term will remain and make the compounds 2D ferromagnets [16].

At high temperature (>150 K), the Mn^{IV}/Ni^{II} ordered clusters exert ferromagnetic fields showing straight lines in the $1/\chi - T$ plots of all the compounds. The effective magnetic moments obtained from fitting to the Curie–Weiss law gave values close to those of corresponding Sr analogues; these values are best explained with the oxidation states Mn^{IV} and Ni^{II}.

Table 3
$1s \rightarrow 3d$ transition energies of Mn and Ni atoms in $Ln_2Ca_2MnNiO_8$ compounds

Compound	Mn K-edge energy (eV)	Ni K-edge energy (eV)
Mn_2O_3	6539.5	
MnO_2	6540.0	
Ca_2MnO_4	6540.0	
$LaMn_{0.5}Ni_{0.5}O_3$	6539.9	8332.0
$Pr_2Ca_2MnNiO_8$	6540.0	8332.8
$Nd_2Ca_2MnNiO_8$	6540.1	8332.4
$Sm_2Ca_2MnNiO_8$	6540.0	8332.2
$Gd_2Ca_2MnNiO_8$	6539.9	8332.4
NiO		8332.1
$LaSrNiO_4$		8332.9
NiOOH		8333.0

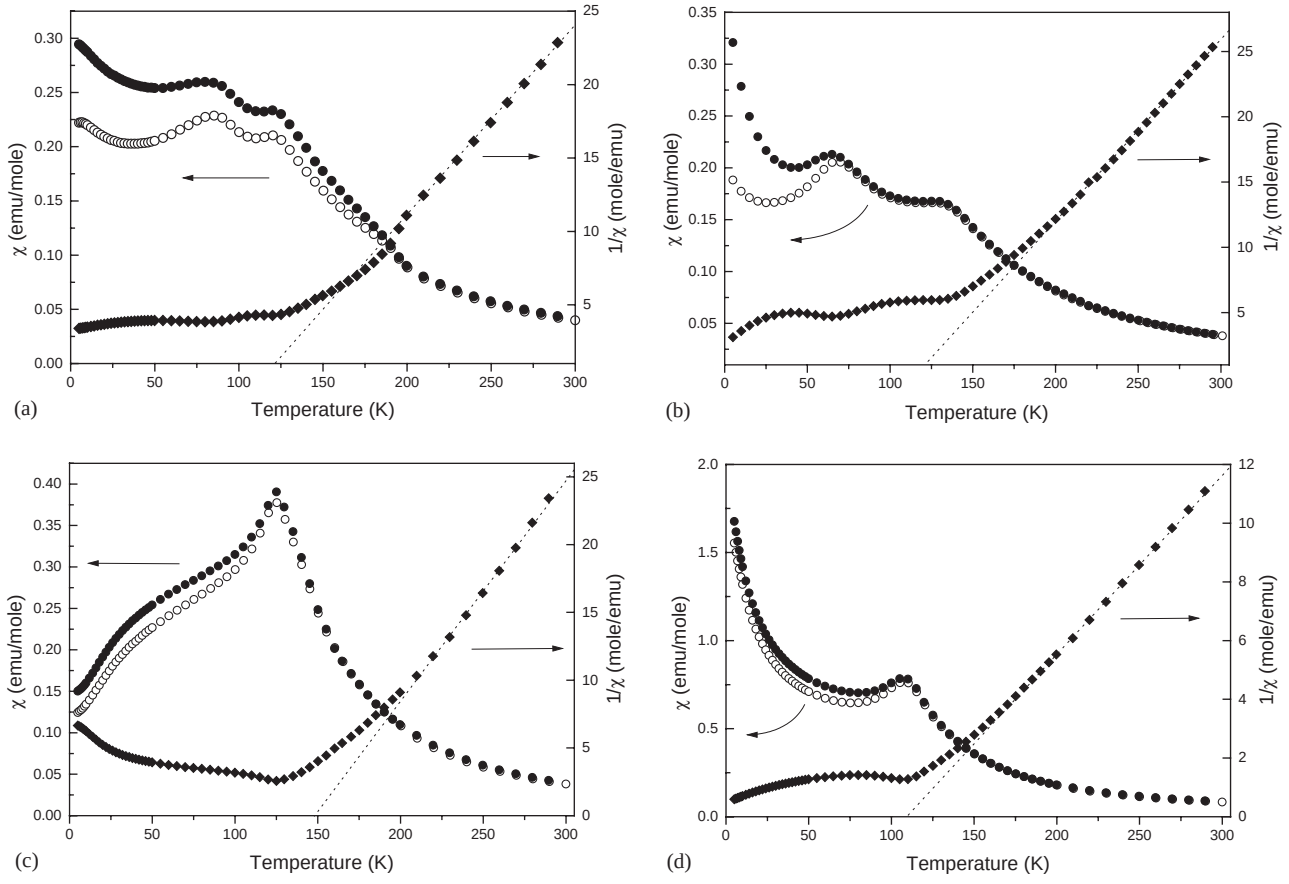

Fig. 6. Magnetic data of (a) $Pr_2Ca_2MnNiO_8$, (b) $Nd_2Ca_2MnNiO_8$, (c) $Sm_2Ca_2MnNiO_8$, and (d) $Gd_2Ca_2MnNiO_8$ compounds. The Curie–Weiss fitting results are shown as dotted lines. FC and ZFC data are shown with filled and open circles, respectively.

Table 4
Summary of magnetic data of $Ln_2Sr_2MnNiO_8$ (Ln = La, Pr, Nd, Sm, Gd) and $Ln_2Ca_2MnNiO_8$ (Ln = Pr, Nd, Sm, Gd) compounds

Compound	T_N (K)		Magnetic moment[b]	Weiss temperature[b] (K)
	Interlayer[a]	Intralayer[a]		
LaCa/LaSr	—/—	—/115	—/3.92	—/123
PrCa/PrSr	80/78	120/111	5.55/5.28	115/78
NdCa/NdSr	65/80	130/116	5.47/4.97	123/84
SmCa/SmSr	12-100/20-60	125/126	4.84/4.64	153/67
GdCa/GdSr	—/10	110/105	7.99/8.21	113/46

[a] See text for definition.
[b] Calculated from the Curie–Weiss fits of high temperature data.

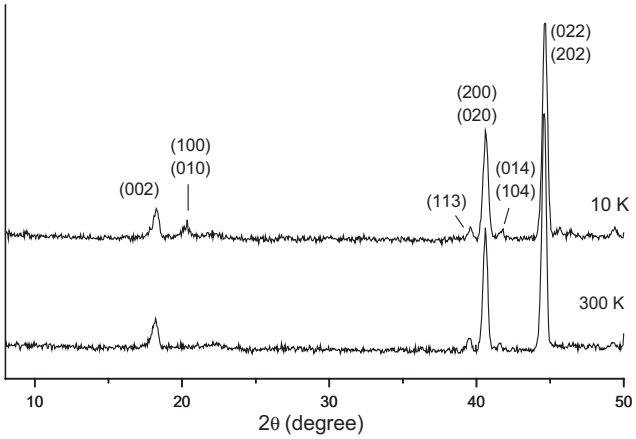

Fig. 7. Neutron diffraction patterns of $Nd_2Ca_2MnNiO_8$ at 300 and 10 K.

However, the Weiss temperatures of the Ca compounds are all significantly higher than those in the Sr-ones. The increased Weiss temperatures may imply that the ferromagnetic fields in the Ca-series are stronger than those in the Sr-series, which, probably, is a consequence of shortened axial M–O bond distances. The buckling of the MO_2 plane may reduce the ferromagnetic field strength but, apparently, its influence is weaker than the bond distances. As the temperature is lowered to 110–130 K, the antiferromagnetic interactions between these clusters through Mn^{IV}–O–Mn^{IV} and/or Ni^{II}–O–Ni^{II} superexchanges set in for all the compounds. This global antiferromagnetic interaction is 2D in nature. Because of the competition between the ferromagnetic and antiferromagnetic superexchange interactions of disordered Mn^{IV} and Ni^{II} ions, the $La_2Sr_2MnNiO_8$ compound in our previous paper showed a spin-glass or frozen spin-like behavior below this temperature with a discrepancy between the ZFC and FC data. The ferromagnetic clusters can have additional interactions provided there are magnetic Ln ion between them. This is what is seen in the magnetic data of Pr and Nd compounds that show second optimum peaks in the $\chi - T$ plots at 80 and 65 K, respectively. The local interaction mode may be expressed as M–O–Ln–O–M. However, the M ions here are not single atoms or a part of a long-range ordered magnetic structure; they represent the ferromagnetic clusters with large magnetic momentum of neighboring MO_2 layers. Therefore, the ferromagnetic clusters of these compounds have two independent antiferromagnetic interactions between them; intralayer interactions through Mn^{IV}–O–Mn^{IV} and/or Ni^{II}–O–Ni^{II} bonds and interlayer interactions through M–O–Ln–O–M bonds. This second ordering is further verified by the low temperature neutron diffraction of the Nd compound that shows a magnetic peak at $2\theta = 20°$ that may be assigned to (100) or (010) peaks (Fig. 7). Unfortunately, because there is only one weak peak, we could not determine the magnetic structure.

From a study on $Ln_{0.7}Sr_{1.3}MnO_4$ single crystals, Hong et al. reported that Ln = Pr and Nd compounds exhibited anisotropic coupling in the c-direction, while the Ln = La compound does not show such effect [4]. They discussed that the Pr and Nd ions between the MnO_2 layers induced interlayer magnetic couplings. These results are in the same line with our observations in that the Pr and Nd ions mediate interlayer magnetic interactions in layered compounds. However, our previous and present data also suggest that the interlayer magnetic interactions are influenced by the strength of magnetic field developed inside the interacting layers.

The implication of our data is that when there is strong enough magnetic field developed in the individual layers, the layers can interact magnetically through the magnetic ions in the interlayer spaces. This does not contrast to the well-established fact that the inner f electrons of the rare earths do not interact strongly, however. The strong intralayer magnetic field is a prerequisite for this phenomenon to occur, and most of the time such conditions are hard to meet. On the other hand, this observation suggests that the similar mechanism holds for the related layered CMR manganites of the general formula $Ln_{2-2x}Sr_{1+2x}Mn_2O_7$ [22]. The Ln = La compounds show a panorama of physical properties as a function of doping level ranging from antiferromagnetic to ferromagnetic and from insulator to metallic [23]. On the contrary, other Ln ions apparently destroy the long-range interactions. Many authors have attributed this contrast between the La and other Ln compounds to the smaller sizes of other Ln ions than La that give rise to localization of the conduction electrons. In addition, our findings suggest that the magnetic Pr and Nd ions induce local antiferromagnetic interactions that compete with the long-range ferromagnetism from the double exchange interaction between the Mn ions. The competition results in the destruction of the long-range double-exchange interactions and the materials become non-metallic and non-ferromagnetic.

In conclusion, we have synthesized a new series of layered compounds $Ln_2Ca_2MnNiO_8$ (Ln = Pr–Gd). These compounds have distorted structures from the ideal tetragonal K_2NiF_4 type structure. The degree of deviation increases with the decrease of Ln ion size. Despite the structural distortions, these compounds show the same magnetic properties as the Sr-analogues of corresponding Ln ions with global antiferromagnetism and rather strong ferromagnetic fields.

Acknowledgments

We thank KRF(2002-015-CP0192) for the financial support and KBSI for the SQUID facility.

References

[1] J.G. Bednorz, K.A. Müller, Z. Phys. B 64 (1986) 189.
[2] (a) E.O. Chi, W.S. Kim, C.S. Hong, N.H. Hur, Y.N. Choi, Bull. Kor. Chem. Soc. 24 (2003) 573;
(b) A. Maignan, C. Martin, G. Van Tendeloo, M. Hervieu, B. Raveau, J. Mater. Chem. 8 (1998) 2411.
[3] (a) W. Bao, C.H. Chen, S.A. Carter, S.-W. Cheong, Solid State Commun. 98 (1996) 55;
(b) B.J. Sternlieb, J.P. Hill, U.C. Wildgruber, G.M. Luke, B. Nachumi, Y. Moritomo, Y. Tokura, Phys. Rev. Lett. 76 (1996) 2169.
[4] C.S. Hong, W.S. Kim, E.O. Chi, N.H. Hur, T.N. Choi, Chem. Mater. 14 (2002) 1832.
[5] J.-H. Choy, S.-J. Kwon, G.-S. Park, Science 280 (1998) 1589.
[6] (a) J.M. Wheatly, T.C. Hsu, P.W. Anderson, Nature 333 (1988) 121;
(b) D.R. Harshman, A.P. Mills, Phys. Rev. B 45 (1992) 10684.
[7] M. Varela, D. Arias, Z. Sefrioui, C. Leon, C. Ballesteros, S.J. Pennycook, J. Santamaria, Phys. Rev. B 66 (2002) 134517.
[8] C.R. Michel, R. amigo, N. Casan-Pastor, Chem. Mater. 11 (1999) 195.
[9] K. Hong, Y.-U. Kwon, D.-K. Han, J.-S. Lee, S. Kim, Chem. Mater. 11 (1999) 1921.
[10] J. Rodriguez-Carvajal, Program: Fullprof (Version 3.2 Jan97-LLB-JRC), Laboratoire Leon Brillouin (CEA-CNRS) (1997).
[11] W.T. Fu, D. Visser, D.J.W. Ijdo, J. Solid State Chem. 169 (2002) 208.
[12] W. Paulus, A. Cousson, G. Dhalenne, J. Berthon, A. Revcolevschi, S. Hosoya, W. Treutmann, G. Heger, R. Le Toquin, Solid State Sci. 4 (2002) 565.
[13] J.A. McAllister, J.P. Attfield, Phys. Rev. B 66 (2002) 014514.
[14] J. Rodriguez-Carvajal, M.T. Fernandez-Diaz, J.L. Martinez, J. Phys.: Condens. Matter 3 (1991) 3215.
[15] A. Daoudi, G. Le Flem, J. Solid State Chem. 2 (1972) 57.
[16] J.B. Goodenough, Magnetism and the Chemical Bond, Wiley, New York, 1963, pp. 168–183.
[17] J. Wong, F.W. Lytle, R.P. Messmer, D.H. Maylotte, Phys. Rev. B 30 (1984) 5596.
[18] R.S. Liu, L.Y. Jang, J.M. Chen, Y.C. Tsai, Y.D. Hwang, R.G. Liu, J. Solid State Chem. 128 (1997) 326.
[19] C. Casan-Pastor, C.R. Zinck, E.M. Michel, G. Tejada-Rosales, Torres-Gomez, Chem. Mater. 13 (2001) 2118.
[20] J.C. Burley, P.D. Battle, P.J. Gaskell, M.J. Rosseinsky, J. Solid State Chem. 168 (2002) 202.
[21] G. Blasse, J. Phys. Chem. Solids 26 (1965) 1969.
[22] N.H. Hur, J.-T. Kim, K.H. Yoo, Y.K. Park, J.C. Park, E.O. Chi, Y.-U. Kwon, Phys. Rev. B 57 (1998) 10740.
[23] Y.-H. Choi, S.-H. Kim, Y.-U. Kwon, C.-H. Lee, J.-S. Lee, H.-S. Shim, J. Kor. Phys. Soc. 42 (2003) 522.